# Adsorption and Dissociation of O₂ on Pt−Co and Pt−Fe Alloys

Ye Xu,[†] Andrei V. Ruban,[‡] and Manos Mavrikakis*,[†]

*Contribution from the Department of Chemical and Biological Engineering, University of Wisconsin−Madison, Madison, Wisconsin 53706, and Center for Atomic-scale Materials Physics, Department of Physics, Technical University of Denmark, DK-2800 Lyngby, Denmark*

Received December 14, 2003; E-mail: manos@engr.wisc.edu

***Abstract:*** Self-consistent periodic density functional theory calculations (GGA-PW91) have been performed to study the adsorption of O and O₂ and the dissociation of O₂ on the (111) facets of ordered Pt₃Co and Pt₃Fe alloys and on monolayer Pt skins covering these two alloys. Results are compared with those obtained on two Pt(111) surfaces, one at the equilibrium lattice constant and the other laterally compressed by 2% to match the strain in the Pt alloys. The absolute magnitudes of the binding energies of O and O₂ follow the same order in the two alloy systems: Pt skin < compressed Pt(111) < Pt(111) < Pt₃Co(111) or Pt₃Fe(111). The reduced activity of the compressed Pt(111) and Pt skins for oxygen can be rationalized as being due to the shifting of the d-band center increasingly away from the Fermi level. We propose that an alleviation of poisoning by O and enhanced rates for reactions involving O may be some of the reasons why Pt skins are more active for the oxygen reduction reaction in low-temperature fuel cells. Finally, a linear correlation between the transition-state and final-state energies of O₂ dissociation on monometallic and bimetallic surfaces is revealed, pointing to a simple way to screen for improved cathode catalysts.

## Introduction

In recent years, a number of platinum−base metal (Pt−M) alloys have been demonstrated to possess greater activity than pure Pt for catalyzing the oxygen reduction reaction (ORR) in acidic electrolytes, which is one of the primary electrochemical reactions in low-temperature fuel cells. Reported enhancements vary from 2−3[1−3] to 10−25 times.[4,5] Typically, one of the 3d transition metals (chromium (Cr), iron (Fe), cobalt (Co), or nickel (Ni)) is used at an atomic concentration of less than 50%. It is uncertain, however, why these alloy catalysts have superior ORR activity. To date, a number of factors that are modified by alloying have been identified. For instance, it has been shown that upon alloying the Pt−Pt distance invariably contracts because the base metal atoms are smaller than Pt atoms.[1] In addition, the formation of so-called "Pt skins," i.e., almost zero base metal content in the outer layers of Pt−M alloy particles, has been observed for Pt−Fe, Pt−Co, and Pt−Ni catalysts. This occurs probably because the base metals tend to leach out of the alloys during operation in acidic electrolytes, while Pt atoms

are redeposited and rearranged on the surface.[5−8] Pt skins can also be formed by annealing the alloys at high temperatures[3,9] because Pt atoms have a strong tendency to segregate to the surface when alloyed with most other transition metals.[10] This is usually accompanied by a simultaneous Pt depletion in the second layer.[11] Still, what aspect of the ORR mechanism is affected by Pt−M alloy catalysts remains unclear. Several researchers have concluded that modified chemisorption of various intermediates is the key to enhanced activity.[1,12] Some have hypothesized that the electronic structures of the Pt skin layers are altered by the underlying alloy substrates, which in turn modifies the facility of electron transfer to O₂.[5]

Here we present a self-consistent periodic density functional theory (DFT) study on the adsorption of O and O₂ and the dissociation of O₂ on Pt−Co and Pt−Fe alloys and respective Pt skin structures. Because methanol crossover is still a problem in direct methanol fuel cells and because methanol can be electrooxidized to CO that could poison the cathode under some conditions,[13] we have also briefly studied CO adsorption on the same surfaces. By comparing the results with corresponding

* To whom correspondence should be addressed.
† University of Wisconsin−Madison.
‡ Technical University of Denmark.

(1) Mukerjee, S.; Srinivasan, S.; Soriaga, M.; McBreen, J. *J. Electrochem. Soc.* **1995**, *142*, 1409.
(2) Paulus, U. A.; Wokaun, A.; Scherer, G. G.; Schmidt, T. J.; Stamenkovic, V.; Radmilovic, V.; Markovic, N. M.; Ross, P. N. *J. Phys. Chem. B* **2002**, *106*, 4181.
(3) Stamenkovic, V.; Schmidt, T. J.; Ross, P. N.; Markovic, N. M. *J. Phys. Chem. B* **2002**, *106*, 11970.
(4) Toda, T.; Igarashi, H.; Watanabe, M. *J. Electroanal. Chem.* **1999**, *460*, 258.
(5) Toda, T.; Igarashi, H.; Uchida, H.; Watanabe, M. *J. Electrochem. Soc.* **1999**, *146*, 3750.
(6) Watanabe, M.; Tsurumi, K.; Mizukami, T.; Nakamura, T.; Stonehart, P. *J. Electrochem. Soc.* **1994**, *141*, 2659.
(7) Igarashi, H.; Fujino, T.; Zhu, Y.; Uchida, H.; Watanabe, M. *Phys. Chem. Chem. Phys.* **2001**, *3*, 306.
(8) Wan, L.-J.; Moriyama, T.; Ito, M.; Uchida, H.; Watanabe, M. *Chem. Commun.* **2002**, 58.
(9) Atli, A.; Abon, M.; Beccat, P.; Bertolini, J. C.; Tardy, B. *Surf. Sci.* **1994**, *302*, 121.
(10) Ruban, A. V.; Skriver, H. L.; Nørskov, J. K. *Phys. Rev. B* **1999**, *59*, 15990.
(11) Gauthier, Y.; Baudoing-Savois, R.; Bugnard, J. M.; Bardi, U.; Atrei, A. *Surf. Sci.* **1992**, *276*, 1.
(12) Arenz, M.; Schmidt, T. J.; Wandelt, K.; Ross, P. N.; Markovic, N. M. *J. Phys. Chem. B* **2003**, *107*, 9813.
(13) Adzic, R. Private communication.

findings on two pure Pt surfaces (one with the equilibrium lattice constant and one compressed by 2%, for reasons to be explained in the Methods) and analyzing surface electronic and geometric structures, we demonstrate that the properties of the Pt skins are substantially modified compared to those of pure Pt, and that the effects can be attributed to the compressive strain imposed by the alloy substrates and to the intermetallic bonding with the base metals in the substrates. Finally, we show that a linear correlation exists between the energy of the transition state of $O_2$ dissociation and the energy of atomic oxygen on a number of monometallic and alloy surfaces.

## Methods

The spin-polarized first-principles total energy calculations are performed using an ultrasoft pseudopotential[14] method as implemented in the DACAPO code.[15] The ordered $Pt_3Co$ and $Pt_3Fe$ phases are chosen to represent Pt−Co and Pt−Fe alloys because they are thermodynamically stable up to high temperatures.[16] There have been reports indicating that disordered $Pt_3M$ alloys[6] or higher base metal contents[2,5] are more active than the ordered phases, but the goal of this study is to investigate not the optimal alloy composition but possible reasons for enhanced activity. Since Pt, $Pt_3Co$, and $Pt_3Fe$ all have the fcc crystal structure, they are all modeled by the thermodynamically most stable (111) facet. The Pt skins are modeled by a single epitaxial layer of Pt on top of $Pt_3Co(111)$ or $Pt_3Fe(111)$ substrate. The thickness of Pt skins on the cathodes of realistic fuel cell systems is not known with certainty, but it probably never exceeds a few layers.[3,7,11] Because the ordered $Pt_3Co$ phase has a lattice constant of 3.85 Å[17] and the ordered $Pt_3Fe$ phase has a lattice constant of 3.87 Å,[18] which represent a ca. 2% and 1.5% contraction, respectively, compared to Pt at the equilibrium lattice constant (3.92 Å),[19] a 2%-compressed pure Pt(111) surface is included to identify strain effects. The 2% compressive strain is applied parallel to the exposed surface while the thickness of the slab is preserved. This approach has been shown to yield accurate estimates of binding energies on strained transition-metal surfaces.[20−22] All slabs are constructed from (2 × 2) surface unit cells, and each slab consists of four layers of metal atoms with the top two layers relaxed. Successive slabs in the *z* direction are separated by a vacuum region equivalent to six metal layers, which correspond to a distance of ~14 Å. Adsorption is allowed on only one of the two sides of each slab with the electrostatic potential adjusted accordingly.[23] The model systems are shown in Figures 1 and 2.

It should be noted that the model adsorption systems in this study resemble single-crystal surfaces exposed to gas-phase oxygen and not the conditions under which the cathode catalyst of a fuel cell operates, where the structure and surface composition of catalyst particles may be much different and where reactivity can be influenced by field effects and the presence of water. Nonetheless, we believe that insights derived from gas−solid interface studies can capture important trends in reactivity, as has been shown recently.[24]

The Kohn−Sham equations are solved self-consistently for the corresponding valence states (O(2s2p), Fe(3d4s), Co(3d4s), and Pt-
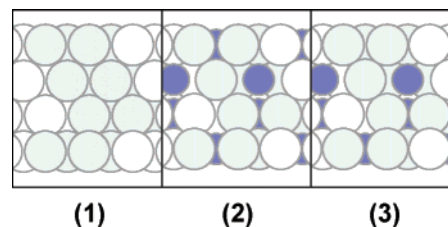
(14) Vanderbilt, D. *Phys. Rev. B* **1990**, *41*, 7892.
(15) Hammer, B.; Hansen, L. B.; Nørskov, J. K. *Phys. Rev. B* **1999**, *59*, 7413.
(16) Hansen, M.; Anderko, K. *Constitution of binary alloys*, 2nd ed.; MaGraw-Hill: New York, 1958.
(17) Kootte, A.; Haas, C.; de Groot, R. A. *J. Phys.: Condens. Matter* **1991**, *3*, 1133.
(18) Tohyama, T.; Ohta, Y.; Shimizu, M. *J. Phys.: Condens. Matter* **1989**, *1*, 1789.
(19) Wyckoff, R. W. G. *Crystal Structures*, 2nd ed.; Wiley: New York, 1963; Vol. 1.
(20) Mavrikakis, M.; Hammer, B.; Nørskov, J. K. *Phys. Rev. Lett.* **1998**, *81*, 2819.
(21) Xu, Y.; Mavrikakis, M. *Surf. Sci.* **2001**, *494*, 131.
(22) Wintterlin, J.; Zambelli, T.; Trost, J.; Greeley, J.; Mavrikakis, M. *Angew. Chem., Int. Ed.* **2003**, *42*, 2850.
(23) Neugebauer, J.; Scheffler, M. *Phys. Rev. B* **1992**, *46*, 16067.
(24) Christoffersen, E.; Liu, P.; Ruban, A. V.; Skriver, H. L.; Nørskov, J. K. *J. Catal.* **2001**, *199*, 123.

**Figure 1.** Cross-section view of model slabs: (1) Pt(111) and 2%-compressed Pt(111), (2) $Pt_3Co(111)$, and (3) monolayer Pt skin on $Pt_3Co$-(111). Large circles represent Pt atoms, and small blue circles represent Co atoms. Pt atoms in the unit cells are colored gray.
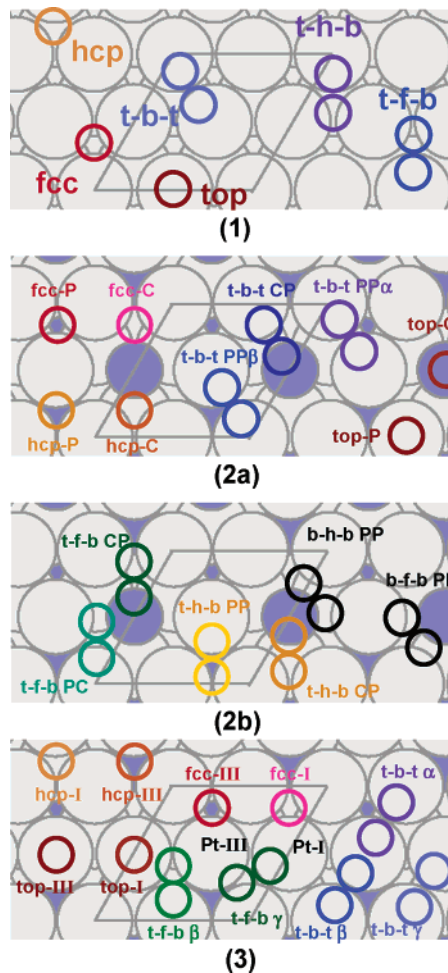


**Figure 2.** Top view of the adsorption sites identified for O and $O_2$ on (1) Pt(111) and 2%-compressed Pt(111), (2a,b) $Pt_3Co(111)$, and (3) monolayer Pt skin on $Pt_3Co(111)$. Large gray circles represent Pt atoms, medium blue circles represent Co atoms, and small open circles represent O atoms, the colors of which match those of the site labels. The unit cell of each surface is delineated.

(6s5d)) in the plane wave basis up to 25 Ry. The exchange-correlation energy and potential are described by the generalized gradient approximation (GGA-PW91).[25,26] The self-consistent PW91 density is determined by iterative diagonalization of the Kohn−Sham Hamiltonian, Fermi population of the Kohn−Sham states ($k_BT = 0.1$ eV), and Pulay mixing of the resultant electronic density.[27] All total energies are extrapolated to $k_BT = 0$ eV. For our slab calculations, the surface Brillouin zone is sampled at 18 special Chadi−Cohen *k* points, which has been verified to ensure the convergence of calculated binding energies for similar systems.[21,28,29]

(25) Perdew, J. P.; Chevary, J. A.; Vosko, S. H.; Jackson, K. A.; Pederson, M. R.; Singh, D. J.; Fiolhais, C. *Phys. Rev. B* **1992**, *46*, 6671.
(26) White, J. A.; Bird, D. M. *Phys. Rev. B* **1994**, *50*, 4954.

The 3d base metals and their alloys with Pt, if the base metals are present at a nonnegligible concentration, are in fact all magnetic. The ordered $Pt_3Co$ phase crosses from the ferromagnetic state into the paramagnetic state at ∼470 K,[16] its Curie temperature. The ordered $Pt_3Fe$ phase is antiferromagnetic at the lowest temperatures and becomes paramagnetic at ∼110 K when the order of the direction of the magnetic moments of Fe atoms is lost. Deviations from the perfect $Pt_3Fe$ phase may produce an intermediate ferromagnetic state or prevent the formation of the antiferromagnetic state.[30] Although current spin density functional theory methods can explicitly treat atoms with randomly oriented spins such as encountered in the paramagnetic state, such calculations are impractical because they demand the use of very large unit cells. In the case of $Pt_3Fe$, however, there is no need to treat the magnetic state of the Fe sublattice exactly. It is clear from a very low magnetic transition temperature that the intersite exchange magnetic interactions, which determine the magnetic structure, are small in $Pt_3$-Fe and should not affect the interatomic interactions. In fact, we have calculated the exchange interaction parameters of the classical Heisenberg Hamiltonian[31] and found that the strongest parameters were 4.9 and 8.8 meV for the first two coordination shells, which are almost an order of magnitude less than the exchange interaction parameters of the bcc Fe lattice (see, for instance, ref 32).

What is more important is the fact that the local electronic structure of Fe atoms is practically independent of the magnetic configuration. In particular, the local magnetic moment of Fe in the collinear disordered local moment state (DLM, which describes the paramagnetic high-temperature state) and in the ferromagnetic state, obtained in the Korringa–Kohn–Rostocker calculations in the atomic sphere approximation and the coherent potential approximation (for the details of the method, see ref 33), are effectively the same: 3.24 and 3.22 $\mu_B$. Besides, the difference in the positions of the d-band center of the ferromagnetic and DLM states is only 3 meV for the majority band and 30 meV for the minority band, which means that the chemical reactivity of Fe atoms in both states should be practically the same. Indeed the binding energy of atomic oxygen on an antiferromagnetic slab is calculated to be almost identical to that on a ferromagnetic slab and independent of the spin orientation of the Fe atom to which the O atom is bonded. On the basis of these findings, we conclude that the use of a ferromagnetic slab, while appropriate for the $Pt_3Co$ phase because it has a relatively high Curie temperature, would also be a very good approximation for the $Pt_3Fe$ phase in the paramagnetic state.

For the ferromagnetic $Pt_3Co$ phase the calculated lattice constant is 3.92 Å, in good agreement with the experimental value of 3.85 Å.[17] The magnetic moments on Co and Pt atoms in ferromagnetic bulk $Pt_3$-Co have been determined with neutron diffraction measurements to be 1.64 and 0.26 $\mu_B$, respectively.[34] Our calculations for bulk $Pt_3Co$ give 1.84 and 0.16 $\mu_B$ as the magnetic moments on Co and Pt, which are due to the valence d electrons. The lattice constant of the ferromagnetic $Pt_3Fe$ phase is calculated to be 3.94 Å, whereas the experimental lattice constant is 3.87 Å.[18] The calculated bulk magnetic moments for $Pt_3Fe$ are 3.21 $\mu_B$ on Fe atoms and 0.28 $\mu_B$ on Pt atoms. Experimentally the antiferromagnetic phase is found to have 3.3 $\mu_B$ on Fe atoms and none on Pt atoms.[30] The calculated equilibrium PW91 lattice constant for bulk Pt is 4.00 Å, in good agreement with the experimental value of 3.92 Å.[19]

A fully relaxed gas-phase $O_2$ molecule is found to have a bond energy of 5.64 eV and a bond length of 1.24 Å, in reasonable agreement with the experimental values of 5.23 eV[35] and 1.21 Å.[36] The PW91 bond energy of gas-phase $O_2$ (5.64 eV) differs from the corresponding number given in ref 35 (6.20 eV) probably because the latter result was obtained with the O–O bond fixed at its experimentally determined length.

The binding energies ($E_b = E_{total} - E_{substrate} - E_{gas-phase\,adsorbate}$), geometries, and magnetic moments of adsorbed O and $O_2$ as well as $O_2$ dissociation paths are explored on the relaxed (111) surfaces. The minimum-energy paths for $O_2$ dissociation are determined using the climbing-image nudged elastic band (cNEB) method.[37] The dissociation of an $O_2$ molecule would yield two O atoms per unit cell, but we designate the atomic state, i.e., when the two O atoms have diffused away from each other, leaving only one per unit cell, to be the final state of the dissociation process. Complete paths shown in the figures below are interpolated[38] by fitting a cubic polynomial through all images on each path guided by the force tangent to the reaction coordinate at each image. Once a minimum-energy path is determined, the transition state is located and the activation energy is calculated as $E_a = E_b^{TS} - E_b^{IS}$, where $E_b^{TS}$ and $E_b^{IS}$ are binding energies of the transition and initial states, respectively.

## Results and Discussion

**Pt(111).** Atomic and molecular oxygen adsorb in several high-symmetry sites on Pt(111) as identified in panel 1 of Figure 2. The binding energies of O and $O_2$ in these adsorption sites are listed in Table 1. The oxygen/Pt(111) system has been studied before by other groups using periodic DFT calculations.[39–41] For the sake of consistency with respect to calculation parameters we have performed our own calculations for this system. The fcc hollow is the most stable adsorption site for atomic oxygen (−3.88 eV/O), whereas the hcp hollow is less favorable by 0.4 eV. Campbell et al.[42] and Gland et al.[43] estimated from experiments the binding energy of an O atom on Pt(111) to be −3.6 eV/O (relative to a free O atom). We find the top site to be considerably less stable, and an O atom adsorbed on the bridge site would slide off into the adjacent fcc site, suggesting it is not a true minimum in the potential energy surface. This happens on all four surfaces we have studied here, so no bridge site entry is included in Table 1. We are able, however, to estimate from calculations performed on a static Pt(111) surface that the diffusion barrier for O on Pt-(111) is between 0.4 and 0.5 eV, in good agreement with experimental estimates.[44] Among the three di-σ-type molecular oxygen states identified, t−b−t is the most stable (−0.62 eV/$O_2$), much like on the other late 5d transition metals (Ir[28] and Au[29]). The t−b−t and t−f−b states are practically energetically degenerate. The t−b−t state carries 0.6 $\mu_B$ of magnetic moment (compared to 2.0 $\mu_B$ in the gas phase), whereas the t−f−b and t−h−b states have zero magnetic moments.

In a recent theoretical study, Gross et al. have shown that $O_2$ dissociation on Pt(111) must always proceed via a molecular precursor state,[45] which demonstrates the importance of studying the dissociation of $O_2$ precursors on Pt(111). We have performed

(27) Kresse, G.; Furthmüller, J. *Comput. Mater. Sci.* **1996**, *6*, 15.
(28) Xu, Y.; Mavrikakis, M. *J. Chem. Phys.* **2002**, *116*, 10846.
(29) Xu, Y.; Mavrikakis, M. *J. Phys. Chem. B* **2003**, *107*, 9298.
(30) Bacon, G. E.; Crangle, J. *Proc. R. Soc. London, A* **1963**, *272*, 387.
(31) Liechtenstein, A. I.; Katsnelson, M. I.; Antropov, V. P.; Gubanov, V. A. *J. Magn. Magn. Mater.* **1987**, *67*, 65.
(32) van Schilfgaarde, M.; Antropov, V. P. *J. Appl. Phys.* **1999**, *85*, 4827.
(33) Ruban, A. V.; Skriver, H. I. *Comput. Mater. Sci.* **1999**, *15*, 119.
(34) Menzinger, F.; Paoletti, A. *Phys. Rev.* **1966**, *143*, 365.
(35) Perdew, J. P.; Burke, K.; Ernzerhof, M. *Phys. Rev. Lett.* **1996**, *77*, 3865.
(36) *CRC Handbook of Chemistry and Physics*, 83rd ed.; CRC Press: Boca Raton, FL, 2002.
(37) Henkelman, G.; Uberuaga, B. P.; Jónsson, H. *J. Chem. Phys.* **2000**, *113*, 9901.
(38) Henkelman, G.; Jónsson, H. *J. Chem. Phys.* **2000**, *113*, 9978.
(39) Eichler, A.; Mittendorfer, F.; Hafner, J. *Phys. Rev. B* **2000**, *62*, 4744.
(40) Gambardella, P.; Sljivancanin, Z.; Hammer, B.; Blanc, M.; Kuhnke, K.; Kern, K. *Phys. Rev. Lett.* **2001**, *87*, 056103.
(41) Sljivancanin, Z.; Hammer, B. *Surf. Sci.* **2002**, *515*, 235.
(42) Campbell, C. T.; Ertl, G.; Kuipers, H.; Segner, J. *Surf. Sci.* **1981**, *107*, 220.
(43) Gland, J. L.; Sexton, B. A.; Fisher, G. B. *Surf. Sci.* **1980**, *95*, 587.
(44) Wintterlin, J.; Schuster, R.; Ertl, G. *Phys. Rev. Lett.* **1996**, *77*, 123.
(45) Gross, A.; Eichler, A.; Hafner, J.; Mehl, M. J.; Papaconstantopoulos, D. A. *Surf. Sci.* **2003**, *539*, L542.

**Table 1.** Binding Energies of O and O$_2$ on the Four Surfaces[a]

| | | | Pt skin on Pt$_3$Co(111) | | Pt$_3$Co(111) | |
| | Pt(111) | 2%-compressed Pt(111) | I | III | C | P |
|---|---|---|---|---|---|---|
| **Atomic Oxygen (eV/O)** | | | | | | |
| top | −2.49 | −2.36 | −2.31 | −2.28 | −3.50 | ns |
| hcp | −3.49 | −3.28 | −3.13 | −3.12 | −4.02 | −3.46 |
| fcc | −3.88 | −3.63 | −3.50 | −3.20 | −4.29 | −3.52 |

| | | | Pt skin on Pt$_3$Co(111) | | | Pt$_3$Co(111) | | |
| | Pt(111) | 2%-compressed Pt(111) | α | β | γ | CP | PP | PC |
|---|---|---|---|---|---|---|---|---|
| **Molecular Oxygen (eV/O$_2$)** | | | | | | | | |
| t−b−t | −0.62 | −0.50 | −0.24 | −0.34 | −0.34 | −0.92 | −0.53 −0.65 | (α) (β) |
| t−f−b | −0.61 | −0.46 | ns | −0.25 | −0.28 | −0.92 | ns | −0.77 |
| t−h−b | −0.45 | −0.32 | ns | ns | ns | −0.67 | −0.48 | ns |
| b−f−b | ns | ns | ns | ns | ns | ns | −0.70 | ns |
| b−h−b | ns | ns | ns | ns | ns | ns | −0.63 | ns |

[a] The binding energies of O and O$_2$ are referenced to O$_{(g)}$ and O$_{2(g)}$, respectively. Surface coverage is 1/4 ML for each species. See Figure 2 for site labeling (I, III, C, P, etc.). ns indicates that no stable state is found.

**Table 2.** Summary of O$_2$ Dissociation Paths on Pt(111), 2%-Compressed Pt(111), and Pt Skin on Pt$_3$Co(111)[a]

| surface | IS | $E_{b,IS}$ (eV/O$_2$) | $E_{b,TS}$ (eV/O$_2$) | $E_a$ (eV/O$_2$) |
|---|---|---|---|---|
| Pt(111) | t−b−t | −0.62 | 0.15 | 0.77 |
| 2%-compressed Pt(111) | t−b−t | −0.50 | 0.39 | 0.89 |
| Pt skin on Pt$_3$Co(111) | t−b−t | −0.34 | 0.59 | 0.93 |

[a] The coverage of O$_2$ is 1/4 ML. $E_b$ is the binding energy referenced to O$_{2(g)}$. $E_a$ is the activation energy associated with each path. IS and TS stand for initial state and transition state, respectively.
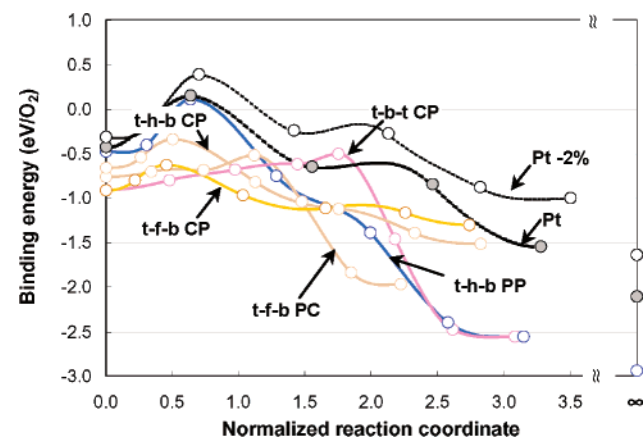


**Figure 3.** Several minimum-energy paths determined by cNEB calculations for O$_2$ dissociation on Pt$_3$Co(111). The paths are labeled by their initial states and correspond to those listed in Table 3. Those colored yellow or red are associated with Co centers, while the dark blue one (t−h−b PP) is associated with Pt centers. The O$_2$ dissociation paths on Pt(111) and 2%-compressed Pt(111) are included as a reference (dashed black curves; the portion between the t−b−t and t−h−b states is omitted). The zero-energy axis corresponds to the total energy of an O$_2$ molecule in the gas phase and the respective clean surfaces at infinite separation. The marked points on each path indicate the positions of the intermediate and end states in cNEB calculations. The points located on the right vertical axis represent the atomic final states ($\theta_O$(111) = 1/4 ML).

cNEB calculations to connect the best initial state (t−b−t) with two oxygen atoms occupying a set of neighboring fcc sites (fcc×2), which represent the best dissociated state. The results are summarized in Table 2, and the interpolated path is included in Figure 3. Snapshots of selected images along the path are shown in Figure 4. The breaking of the O−O bond does not commence until the O$_2$ precursor has rotated over to the neighboring t−h−b site, after which the O−O bond begins to
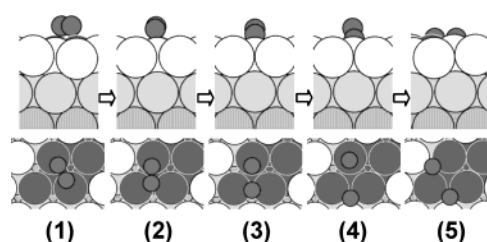


**Figure 4.** Cross-section and top views of selected states along the O$_2$ dissociation path from t−b−t to fcc×2 on unstrained Pt(111): (1) the initial state (t−b−t), (2) a stable intermediate molecular state, t−h−b, (3) the third (transition state) and (4) the fourth intermediate image, and (5) the coadsorption state (fcc×2). For clarity, only one O$_2$ molecule is shown in each panel. The O$_2$ dissociation processes on the compressed Pt(111) and monolayer Pt skin surfaces feature essentially identical transformation of the O$_2$ molecule.

stretch in place. The activation energy is 0.77 eV with respect to the t−b−t state or 0.60 eV with respect to the t−h−b state. The transition state is located 0.15 eV above the gas-phase zero and can be described as a bridge + top configuration (panel 3 of Figure 4). Our results agree closely with those of Hafner and co-workers[39] ($E_b$(t−b−t) = −0.72 eV; $E_a$ = 0.9 eV) and Hammer and co-workers[40,41] ($E_b$(t−b−t) = −0.6 eV; $E_a$ = 0.7 eV). Experimentally, the heat of adsorption of the precursor state on Pt(111) has been estimated at −0.38 eV, and the activation energy for the dissociation of the precursor has been estimated at 0.34 eV.[43,46] The disagreement between the measured and calculated $E_a$ values may be due to the fact that the previous DFT studies and this one have been carried out for high surface coverage (1/4 monolayer (ML) of O$_2$ dissociating into 1/2 ML of O). Furthermore, surface defects and a host of other factors may have also had an effect on the experimentally derived estimates.

**Effect of Strain: Compressed Pt(111).** The same set of atomic and molecular adsorption sites are found on the 2%-compressed Pt(111) surface as on Pt(111) at the equilibrium lattice constant. Consistent with previous findings,[20,21] a 2% compressive strain in the surface destabilizes the adsorption of both atomic and molecular oxygen. At 1/4 ML coverage the magnitude of the binding energy of atomic oxygen in 3-fold hollows is reduced by ∼0.2 eV/O, and the oxygen atom is located ∼0.2 Å higher above the surface than on the unstrained

(46) Gland, J. L. *Surf. Sci.* **1980**, *93*, 487.

**Table 3.** Summary of Several $O_2$ Dissociation Paths on $Pt_3Co(111)^a$

| reaction center | IS | $E_{b,IS}$ (eV/O₂) | $E_{b,TS}$ (eV/O₂) | $E_a$ (eV/O₂) |
|---|---|---|---|---|
| Co | t−b−t CP | −0.92 | −0.51 | 0.41 |
| Co | t−f−b PC | −0.77 | −0.53 | 0.24 |
| Co | t−f−b CP | −0.92 | −0.64 | 0.28 |
| Co | t−h−b CP | −0.67 | −0.35 | 0.32 |
| Pt | t−h−b PP | −0.48 | 0.10 | 0.58 |

$^a$ The coverage of $O_2$ is 1/4 ML. $E_b$, $E_a$, IS, and TS are as defined in Table 2. See Figure 2 for site nomenclature.

surface. The molecular precursors lose ∼0.1 eV/O₂ in binding energy, but the geometric and magnetic properties of the precursors remain almost unchanged. Because the relative stabilities of the various atomic and molecular adsorption states have not changed, we study the same O₂ dissociation path as we have done on Pt(111) at the equilibrium lattice constant, namely, from t−b−t to fcc×2. The result has essentially identical geometric features (see Figure 4). The difference is mainly in the energetics (see Table 2): Here not only is the transition state destabilized by the compressive strain (now located 0.39 eV above the gas-phase zero), but the activation energy is also increased (0.89 eV with respect to the t−b−t state or 0.71 eV with respect to the t−h−b state), indicating that the destabilization of the transition state is greater in magnitude than that of the molecular initial state.

**Pt₃Co(111): Co Center vs Pt Center.** One-fourth of the atoms in the Pt₃Co(111) surface are Co. The presence of the Co atoms differentiates formerly identical adsorption sites. Three-fourths of the fcc and hcp sites are now located next to a Co atom, and the remaining 1/4 are surrounded by Pt atoms only. There are also two types of top sites, those on a Pt atom and those on a Co atom. As shown in panel 2a of Figure 2, those sites on or near Co atoms are designated as "C" sites (for Co centers) and those not in the vicinity of Co atoms as "P" sites (for Pt centers). The inhomogeneity of the Pt₃Co(111) surface also creates a whole array of possible nonequivalent t−b−t, t−f/h−b, and b−f/h−b O₂ adsorption states (see panels 2a and 2b of Figure 2). The binding energies of the stable atomic and molecular states that we have found on this surface are listed in Table 1. The t−b−t states each have a magnetic moment of ∼0.5 $\mu_B$, the t−f/h−b states each have ∼0.1 $\mu_B$, and the b−f/h−b states each have ∼0.3 $\mu_B$. Compared with O adsorbed on a 2 × 2 × 4 Co(0001) slab (also with the top two layers relaxed), the binding energy of which we have calculated to be −5.44 eV (hcp site preferred) as a reference, Co centers are significantly diluted by neighboring Pt atoms and bind oxygen much more weakly. Therefore, the alloy surface as a whole is capable of binding both O and O₂ much more strongly than Pt(111). Furthermore, the potential energy surfaces for O and O₂ become more corrugated as the adsorption wells for both species are considerably deeper around Co centers.

The multitude of O₂ precursor states on the Pt₃Co(111) surface give rise to a wider array of O₂ dissociation paths than on Pt(111). We have calculated a number of these possible paths using the cNEB method. The results are summarized in Table 3 and depicted in Figure 3. Given the relatively high concentration of Co atoms in the surface, no dissociation path can occur completely away from Co centers. Nonetheless, we choose to associate some of the paths with Pt centers because their initial

and transition states occur over Pt centers, whereas others, in which these key states occur in the vicinity of a Co atom, are associated with Co centers. To find the dissociation path with the lowest barrier requires a complete and exhaustive study of all possible paths. The subset that we have calculated should be, however, sufficient for affording some insights into the reactivity of the surface. From Figure 3 it is clear that the Co-center paths tend to have more stable transition states and smaller activation energies, whereas the Pt-center paths (only one is shown) have less stable transition states and larger activation energies. The Co centers are therefore more reactive than the Pt centers for O₂ dissociation.

**Monolayer Pt Skin on Pt₃Co(111).** When a monolayer of Pt is pseudomorphically laid on Pt₃Co(111), the Pt atoms in the monolayer are differentiated by Co atoms beneath them. In the (2 × 2) unit cell used in this study, three of the surface Pt atoms have a Co nearest neighbor in the second layer (Pt-III, panel 3 of Figure 2) and the fourth Pt atom has only Pt atoms beneath it (Pt-I, same figure). This differentiation has in fact been observed experimentally: Two types of Pt atoms were identified in the pure Pt surface of annealed Pt₈₀Fe₂₀(111) in LEED[47] and in PES (using tunable synchrotron radiation).[48] The different surface Pt atoms create nonequivalent adsorption sites (e.g., fcc, hcp, t−b−t), like on Pt₃Co(111). The difference among the nonequivalent sites of each type of adsorbate configuration is typically less than 0.1 eV, with the only exception being that O prefers the fcc-I site to the fcc-III site by 0.3 eV (see Table 1). The t−b−t O₂ states each have a magnetic moment of ∼0.7 $\mu_B$, whereas the t−f−b states are nonmagnetic.

The most striking feature of the Pt skin surface is that it binds both O and O₂ even more weakly than 2%-compressed Pt(111), the reduction being ∼0.15 eV per O and O₂. The O₂ dissociation path determined by cNEB as having the lowest barrier, which runs from the t−b−t$\beta$ state to a set of adjacent fcc-I sites, shows that the transition state is destabilized by 0.2 eV/O₂ compared to 2%-compressed Pt(111) (see Table 2). The dissociation barrier is therefore higher by 0.04 eV than on 2%-compressed Pt(111). The geometric features of this particular path are nonetheless similar to those on Pt(111), uncompressed or compressed (see Figure 4).

**Cross Comparison of the Four Surfaces.** To compare the adsorption and dissociation of oxygen on these four surfaces, the binding energies of atomic and molecular oxygen states as well as the transition states and activation energies of O₂ dissociation are plotted in Figure 5. The adsorption energies of CO on the four surfaces are also included. Our calculations find that CO prefers the fcc site instead of the experimentally determined top site on Pt(111). This is a known problem with plane wave DFT methods using the GGA.[49] Nonetheless, the binding energy we find for CO adsorbed in the fcc site on Pt-(111) (−1.79 eV) agrees closely with experimental findings of −1.8 eV.[50] A trend similar to those for O and O₂ is observed for CO. Overall, Figure 5 suggests that about half of the lost reactivity of the monolayer Pt skin surface may be attributed

(47) Beccat, P.; Gauthier, Y.; Baudoing-Savois, R.; Bertolini, J. C. *Surf. Sci.* **1990**, *238*, 105.
(48) Barrett, N.; Guillot, C.; Bertolini, J. C.; Massardier, J.; Khanra, B. C. *Surf. Sci.* **1992**, *260*, L11.
(49) Olsen, R. A.; Philipsen, P. H. T.; Baerends, E. J. *J. Chem. Phys.* **2003**, *119*, 4522.
(50) Yeo, Y. Y.; Vattuone, L.; King, D. A. *J. Chem. Phys.* **1997**, *106*, 392.
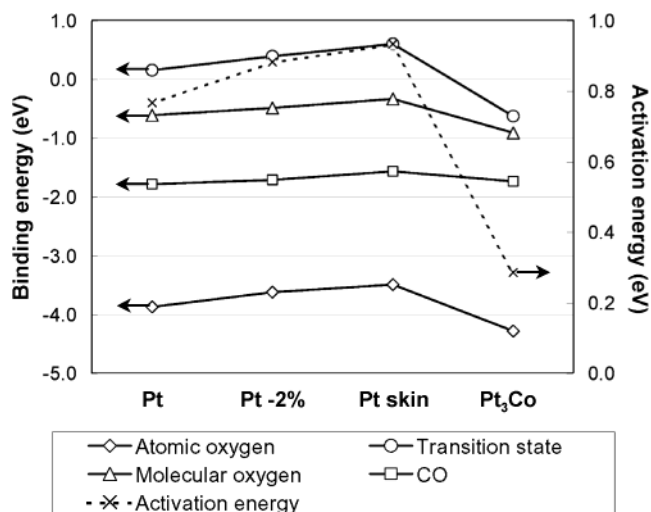
**Figure 5.** Binding energies of $O_{(a)}$, $O_{2(a)}$, and $CO_{(a)}$ and the transition states of $O_2$ dissociation on Pt(111), 2%-compressed Pt(111), Pt skin on Pt$_3$Co-(111), and Pt$_3$Co(111). The corresponding $O_2$ activation energies are also included. The most stable state for each species and the transition state of the dissociation path with the smallest activation energy on each surface are shown. Lines are only guides to the eye.
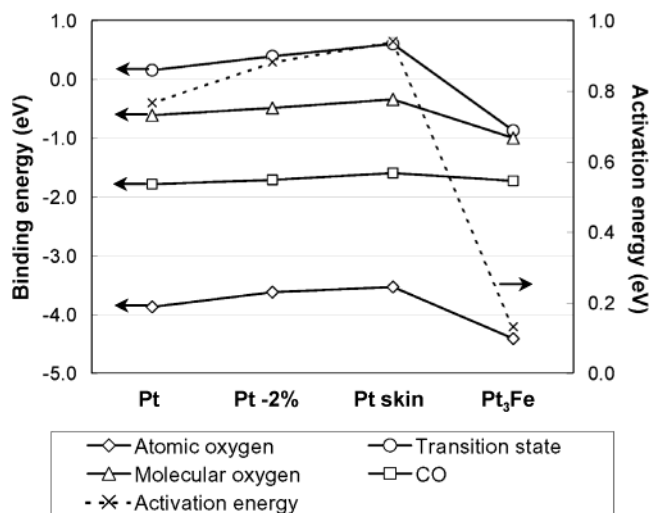


**Figure 6.** Binding energies of $O_{(a)}$, $O_{2(a)}$, and $CO_{(a)}$ and the transition states of $O_2$ dissociation on Pt(111), 2%-compressed Pt(111), monolayer Pt skin on Pt$_3$Fe(111), and Pt$_3$Fe(111). The corresponding $O_2$ activation energies are also included. The most stable states for each species and the transition state of the dissociation path with the smallest activation energy on each surface are shown. Lines are only guides to the eye.

to the effect of compressive strain. Coupling of the Pt skin to the Pt$_3$Co substrate should therefore account for the other half of reactivity loss.

**Pt$_3$Fe(111) and Monolayer Pt Skin on Pt$_3$Fe(111).** Because of the similarities between the Pt$_3$Co and the Pt$_3$Fe systems, we will only summarize the results on Pt$_3$Fe(111) and Pt skin on Pt$_3$Fe(111) for the sake of brevity. The two surfaces are analogous to their Pt$_3$Co counterparts (refer to panels 2 and 3 of Figure 2, with the blue circles now representing Fe atoms). The binding energies and $O_2$ dissociation barriers (see Figure 6) show the same trend as that across Pt$_3$Co and its Pt skin surface; i.e., the Pt skin has a destabilizing effect on the adsorption of O and $O_2$ in addition to what is attributable to compressive strain. The maximum binding energy of O is $-4.42$ eV/O ($-4.47$ eV/O on an antiferromagnetic slab), and the maximum binding energy of $O_2$ is $-1.01$ eV, both about $\sim$0.1

**Table 4.** Summary of Three $O_2$ Dissociation Paths on Pt$_3$Fe(111)[a]

| reaction center | IS | $E_{b,IS}$ (eV/O$_2$) | $E_{b,TS}$ (eV/O$_2$) | $E_a$ (eV/O$_2$) |
|---|---|---|---|---|
| Fe | t–b–t FP | $-0.88$ | $-0.73$ | 0.15 |
| Fe | t–f–b PF | $-0.88$ | $-0.71$ | 0.17 |
| Fe | t–f–b FP | $-1.01$ | $-0.87$ | 0.14 |

[a] The coverage of $O_2$ is 1/4 ML. $E_b$, $E_a$, IS, and TS are as defined in Table 2. See Figure 2 for site nomenclature.

eV stronger than on Pt$_3$Co(111). The cNEB results of three dissociation paths over Fe centers, which are expected to be the most reactive areas on this surface, are listed in Table 4. In general the transition states are more stable, and the activation energies are smaller on Pt$_3$Fe(111) than on Pt$_3$Co(111) ($E_a = 0.14$ eV on the former vs 0.24 eV on the latter). The two Pt skin surfaces are almost identical in reactivity: The difference in binding energy is $\sim$0.04 eV for O and almost none for $O_2$. The barrier to $O_2$ dissociation on Pt skin on Pt$_3$Fe(111) is 0.94 eV (0.93 eV on Pt skin on Pt$_3$Co(111)). The binding energies of CO on Pt$_3$Fe(111) and its skin structure are also almost identical to those on the corresponding Pt$_3$Co surfaces.

**Analyses.** The following analyses apply in most parts to both the Pt$_3$Co and Pt$_3$Fe systems, but to avoid redundancy, we will mention Pt$_3$Co only. We have suggested above that, whereas the Pt$_3$Co(111) surface is clearly much more reactive for oxygen adsorption and dissociation than pure Pt(111) itself, the interaction between the Pt monolayer and the Pt$_3$Co substrate can produce a destabilization of oxygen species in addition to what is attributable to the effect of lattice compression. If the surface of a Pt–Co catalyst is a Pt skin structure rather than an alloy under operating conditions, then enhancement in catalytic performance must be attributed to something other than the ease of $O_2$ dissociation. It is noticeable that, when compared to Pt-(111), the destabilization of O adsorption due to the monolayer Pt skin (0.38 eV/O, Table 1) is about twice as large as the corresponding increase in the activation energy for $O_2$ dissociation (0.16 eV, Table 2). A partial alleviation of the poisoning of the surface by adsorbates such as O could therefore make the difference. In addition, we find that, similar to what has been reported by Sakong et al.[51] for hydrogen on copper, the top site for O on Pt(111) is much less affected by compressive strain than are the 3-fold sites, which suggests that the potential energy surface for O becomes smoother on a compressed surface. As a result, elementary reaction steps in the ORR mechanism that involve the activation of O (or other species if they follow the same trend) across the less coordinated bridge or top sites may become easier on Pt skin, thus facilitating the ORR.

Next we investigate the dynamics of the Pt skin formation on Pt$_3$Co alloy. For this purpose we first obtain the segregation energies and effective interactions,[52,53] which enter into the corresponding configurational Hamiltonian for the segregation problem. Then, using the interactions, we perform Monte Carlo (MC) simulations of a clean Pt$_3$Co(111) surface. We find that, at $T = 400$ K, as long as the overall stoichiometry of the bulk alloy is in the neighborhood of Pt:Co = 3:1, Pt atoms always

(51) Sakong, S.; Gross, A. *Surf. Sci.* **2003**, *525*, 107.
(52) Ruban, A. V.; Simak, S. I.; Korzhavyi, P. A.; Skriver, H. L. *Phys. Rev. B* **2002**, *66*, 024202.
(53) Pourovskii, L. V.; Ruban, A. V.; Abrikosov, I. A.; Vekilov, Y. K.; Johansson, B. *Phys. Rev. B* **2001**, *64*, 035421.

**Table 5.** Several Characteristics of the Electronic and Geometric Structures of the Four Clean Surfaces[a]

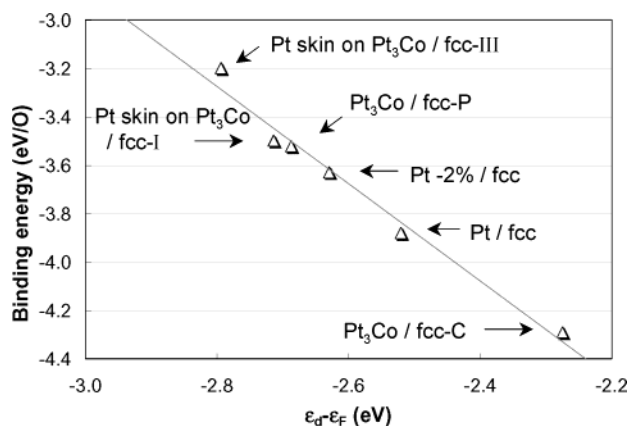| | | $\epsilon_d$ (eV) | $\sigma$ | $f$ (%) | max corrugation of top layer (Å) | min vertical separation b/w Pt atoms in top two layers (Å) |
|---|---|---|---|---|---|---|
| Pt(111) | | −2.52 | 5.93 | 93.3 | 0.00 | 2.33 |
| 2%-compressed Pt(111) | | −2.63 | 6.20 | 93.2 | 0.00 | 2.39 |
| Pt skin on Pt₃Co(111) | Pt-I | −2.58 | 6.14 | 93.4 | 0.10 | 2.32 |
| | Pt-III | −2.79 | 6.13 | 93.3 | | |
| Pt₃Co(111) | Pt | −2.69 | 5.88 | 93.5 | 0.06 | 2.28 |
| | Co | −1.45 | 5.56 | 79.0 | | |
| Co(0001) | | −1.48 | 5.57 | 81.3 | 0.00 | n/a |

[a] Co(0001) is included as a reference. See the text for definitions of the parameters. n/a stands for not applicable.

segregate to the surface and a pure Pt overlayer forms, which agrees with the experimental finding that Pt-only layers form on Pt₃Co or near-Pt₃Co alloys upon annealing.[3,11] This is so because Pt atoms segregate strongly to the surface of Pt−Co alloys (the segregation energy of Pt is about −0.5 eV), but the ordering energy, which could help Co atoms incorporate into the surface layer of this particular facet,[54] is not strong enough. The ordering energy is further suppressed by the ferromagnetism of the Pt₃Co alloy. Our MC simulations show that, if the alloy is confined in the ferromagnetic state, the critical temperature for order ↔ disorder transition is reduced to ∼500 K, significantly lower than the ∼1000 K if the alloy is allowed to cross into the paramagnetic state.

This picture is valid, however, only in the case of a clean Pt₃Co(111) surface. In the presence of O, one has to take into consideration an additional gain of the energy due to the difference in the binding energy of O to Pt and Co atoms on the surface. In particular, the binding energy of O at the Co center of Pt₃Co(111) is ∼0.8 eV greater than that on the monolayer Pt skin, and thus, the gain in O adsorption is sufficient for overcoming the segregation energy (∼0.5 eV) and effecting a countersegregation of Co atoms to the surface, which has been observed experimentally on Pt₃Co(110).[55] Therefore, the adsorption of O and other oxygenated species (such as OH and H₃O⁺) may cause the migration of near-surface Co atoms to the surface. This could in turn lead to the dissolution of the Co atoms and accelerate the formation of Pt skin structures at the cathode of a low-temperature acid−electrolyte fuel cell during operation.

Because the d-band model developed by Hammer and Nørskov[56,57] has been used successfully to explain trends in reactivity of transition-metal and alloy surfaces, we implement it here to explain the activity of the Pt skin surface. Table 5 lists several parameters in the d-band model: $\epsilon_d$, the center of the d band with respect to the Fermi level or the first moment of the d band; $\sigma$, the spread of the d band or its second moment; $f$, the filling of the d band. The overall binding energy of an adsorbate to a transition-metal surface can be decomposed in the following way:

$$E = E_{sp} + E_{d\_hyb} + E_{d\_orth}$$

(54) Ruban, A. V. *Phys. Rev. B* **2002**, *65*, 174201.
(55) An, K. S.; Kimura, A.; Kamakura, N.; Kakizaki, A.; Park, C. Y.; Tanaka, K. *Surf. Sci.* **1998**, *401*, 336.
(56) Hammer, B.; Nørskov, J. K. *Surf. Sci.* **1995**, *343*, 211.
(57) Greeley, J.; Nørskov, J. K.; Mavrikakis, M. *Annu. Rev. Phys. Chem.* **2002**, *53*, 319.



**Figure 7.** Binding energies of atomic O vs d-band centers ($\epsilon_d$) of the four clean surfaces. Labels identify the adsorption sites. The best linear fit is drawn.

$E_{sp}$ comes from the coupling of the adsorbate levels to the metal sp states and is usually the main stabilizing contribution. The next two terms arise from the coupling of the renormalized adsorbate states to the metal d states. $E_{d\_orth}$ is the cost of orthogonalization, which is proportional to $V^2$, the d-band coupling matrix element. $E_{d\_hyb}$ is the gain from hybridization, which is proportional to $V^2/|\epsilon_d - \epsilon_a|$, where $\epsilon_d$ and $\epsilon_a$ are the centers of the metal d band and the renormalized adsorbate states, respectively.[58] According to the analysis of Hammer et al.,[59] *if the change is small* in the adsorbate−surface interaction, one can expect a linear correlation over a small range of $\epsilon_d$:

$$\delta E \approx \frac{V^2}{|\epsilon_d - \epsilon_a|^2} \delta\epsilon_d$$

The binding energies of O on Pt(111), 2%-compressed Pt-(111), Pt skin, and Pt₃Co(111) are plotted against the d-band centers of the corresponding clean surfaces in Figure 7. The first two surfaces consist purely of Pt atoms, so each is characterized by a single $\epsilon_d$. The Pt skin and Pt₃Co(111) surfaces, however, are composed of nonequivalent atoms. For instance, the Pt-III atoms on the Pt skin surface have a d-band center of −2.79 eV, whereas the Pt-I atoms have a d-band center of −2.58 eV (see Table 5). Consequently, although the fcc-III site is surrounded only by Pt-III atoms and may be characterized by the $\epsilon_d$ of the Pt-III atoms, the fcc-I site, on the other hand, is not homogeneous. Following the example set out in ref 60, we have calculated the ratio ($r$) of the quantity $V^2/|\epsilon_d - \epsilon_a|^2$ for Pt on the Pt(111) surface to that for Pt-I and Pt-III atoms on the alloy surface (see ref 61 parameter values):

$$r_{Pt(111)/Pt-I} = \frac{V_{Pt}^2}{|\epsilon_{d,Pt} - \epsilon_a|^2} \Big/ \frac{V_{Pt-I}^2}{|\epsilon_{d,Pt-I} - \epsilon_a|^2} \approx 0.96$$

$$r_{Pt(111)/Pt-III} = \frac{V_{Pt}^2}{|\epsilon_{d,Pt} - \epsilon_a|^2} \Big/ \frac{V_{Pt-III}^2}{|\epsilon_{d,Pt-III} - \epsilon_a|^2} \approx 1.00$$

The results are nearly unity and so should permit us to include

(58) Hammer, B.; Morikawa, Y.; Nørskov, J. K. *Phys. Rev. Lett.* **1996**, *76*, 2141.
(59) Hammer, B.; Nielsen, O. H.; Nørskov, J. K. *Catal. Lett.* **1997**, *46*, 31.
(60) Pallassana, V.; Neurock, M.; Hansen, L. B.; Hammer, B.; Nørskov, J. K. *Phys. Rev. B* **1999**, *60*, 6146.

the fcc-I point in Figure 7 by calculating a $V^2$-weighted $\epsilon_d$[62] for the fcc-I site:

$$\epsilon_{d\_effective} = \frac{2V_{Pt-III}^2\epsilon_{d,Pt-III} + V_{Pt-I}^2\epsilon_{d,Pt-I}}{2V_{Pt-III}^2 + V_{Pt-I}^2} = -2.71$$

The same problem exists for the Pt$_3$Co(111) surface: We are able to include the fcc-P point in Figure 7, but at the Co center because the O atom interacts with disparate Co and Pt d states simultaneously ($r_{Pt(111)/Co\uparrow} = 1.64$; $r_{Pt(111)/Co\downarrow} = 2.32$; see ref 61), a single effective $\epsilon_d$ cannot be calculated according to the spirit of the d-band model. Nevertheless, considering the clear preference of O for the Co center on Pt$_3$Co(111), if we calculate the arithmetic mean of the $\epsilon_d$ values of the three atoms surrounding the fcc-C site and add the corresponding point to Figure 7, we observe that the linear trend is preserved. Apparently, the differences in the reactivity toward O among these sites and surfaces can be rationalized as due mainly to the change in the position of $\epsilon_d$.

The 2% compressive strain noticeably downshifts $\epsilon_d$ ($-2.63$ eV for 2%-compressed Pt(111) vs $-2.52$ eV for Pt(111); see Table 5) because it increases the spread of the d band, a consequence of the Pauli exclusion principle, but does not change the filling of the d band since the slab is still purely Pt. To explain the additional change in $\epsilon_d$ on the Pt skin, we note that the minimum vertical separation between Pt atoms in the top two layers (also in Table 5) is reduced by 0.07 Å in going from 2%-compressed Pt(111) to the Pt skin. Evidently the Pt-III atoms are held much closer to the second layer by the Co atoms beneath than they would be in the absence of the Co atoms. The compressed pure Pt surface can relieve some of its strain by increased separation from the layer beneath it, but this relief is frustrated for the Pt skin by the Co atoms. We also note that the Pt-I atoms in the surface are located 0.10 Å above the Pt-III atoms (the maximum corrugation in Table 5, calculated as the vertical separation between the highest and lowest lying atoms in the surface layer). Somewhat separated from their neighbors, the Pt-I atoms now experience a smaller effective coordination and become somewhat more reactive than the Pt-III atoms (compare the binding energy of O in the fcc-I site with that of O in the fcc-III site in Table 1). Still, the monolayer Pt skin as a whole becomes even less reactive than the 2%-compressed Pt(111). In a recent study[63] of epitaxial Pt layers grown on Ru(0001) Schlapka et al. found that the influence of the Ru substrate decays rapidly with the thickness of the Pt layers and is negligible beyond four Pt monolayers. The compressive strain imposed by the Ru substrate, on the other hand, is relieved more slowly, and it takes 20–30 monolayers for the adsorption properties of CO, the probe molecule, to revert
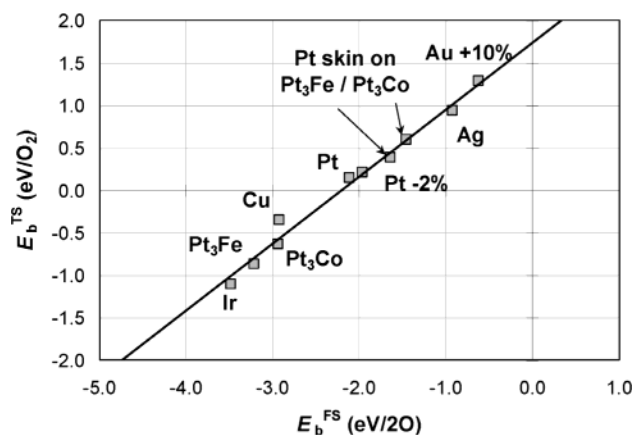


**Figure 8.** Binding energies of the transition states of O$_2$ dissociation ($E_b^{TS}$) vs binding energies of the atomic final states with respect to gas-phase O$_2$ ($E_b^{FS} = 2E_b^O - BE_{O_2(g)}$) on the (111) facets of several fcc transition metals and alloys. If multiple dissociation paths exist on a surface, the one with the most stable transition state is chosen. The result of least-squares linear regression of all the data points is $E_b^{TS} = (0.79 \pm 0.03)E_b^{FS} + (1.73 \pm 0.08)$. $R^2$ is equal to 0.99.

to that of Pt(111) at the equilibrium lattice constant. Therefore, we expect the interlayer Co–Pt interaction to be what further reduces the reactivity of the monolayer Pt skin. This coupling effect would quickly dissipate as the Pt skin grows thicker, and the reactivity of the surface would eventually revert to the 2%-compressed Pt(111) level.

Finally, although the Pt atoms have a diluting effect on the more reactive Co atoms on the Pt$_3$Co(111) surface, the difference between their d-band centers ($-2.69$ eV for Pt and $-1.45$ eV for Co; see Table 5) is in fact widened compared to that of pure Pt(111) ($-2.52$ eV) vs pure Co(0001) ($-1.48$ eV). Lopez and Nørskov have suggested that bimetallic alloys with one magnetic and one nonmagnetic component tend to result in inhomogeneous surfaces with both active and inactive centers.[64] Our results suggest that Pt$_3$Co may belong to this group. We also note that the Pt d-band filling does not change appreciably across the four systems. Alloying Pt with Co seems to result in a slight charge transfer from Co to Pt, which may be attributable to the difference in electronegativity of Pt and Co. For now we cannot reconcile this result with the substantial increase in Pt d-band vacancy previously reported for Pt–M alloys.[1]

**Linear Energy Correlation.** On several close-packed transition-metal surfaces that we have studied so far, including Cu-(111),[21] Ir(111),[28] and 10%-stretched Au(111),[29] as well as Ag(111)[65] and equilibrium and 2%-compressed Pt(111), the energetics of O$_2$ dissociation follows a well-defined trend (see Figure 8), i.e., that there is a linear correlation between the energy of the transition state and the energy of the final atomic state. Furthermore, points corresponding to the alloy surfaces considered in this study, i.e., Pt$_3$Co(111), Pt$_3$Fe(111), and their corresponding skin surfaces, all lie close to the line predicted by the monometallic systems. To our knowledge, this is the first time that a Brønsted–Evans–Polanyi-type correlation for surface reaction[66] was successfully extended to multicomponent systems. This linear correlation between transition-state and

(61) $\epsilon_a$ is the position of the renormalized O 2p state, which is centered at about $-5.5$ eV. $\epsilon_d$ is the center of the Pt d band (see Table 5). $V^2$ is calculated from the LMTO potentials of the O and Pt states and has an inverse dependence on the sixth power of the Pt–O bond length (O is adsorbed in the fcc site). We have calculated $V^2$ to be 60.5 (=4491/2.05$^6$) for Pt-I, 53.9 (=4491/2.09$^6$) for Pt-III, 37.0 for Co$\uparrow$ (spin-up) (=1581/1.87$^6$), and 43.2 for Co$\downarrow$ (spin-down) (=1846/1.87$^6$). The d-band centers for Co$\uparrow$ and Co$\downarrow$ are $-2.45$ and $-0.45$ eV, respectively, on Pt$_3$Co(111). For reference, $V^2$ for equilibrium Pt(111) is 59.1 (=4518/2.06$^6$). For values of $V^2$ for other transition metals, see: Ruban, A. V.; et al. *J. Mol. Catal. A: Chem.* **1997**, *115*, 421.
(62) Pallassana, V.; Neurock, M.; Hansen, L. B.; Nørskov, J. K. *J. Chem. Phys.* **2000**, *112*, 5435.
(63) Schlapka, A.; Lischka, M.; Gross, A.; Käsberger, U.; Jakob, P. *Phys. Rev. Lett.* **2003**, *91*, 016101.

(64) Lopez, N.; Nørskov, J. K. *Surf. Sci.* **2001**, *477*, 59.
(65) Xu, Y.; Greeley, J.; Mavrikakis, M. Manuscript in preparation.
(66) Nørskov, J. K.; Bligaard, T.; Logadottir, A.; Bahn, S.; Hansen, L. B.; Bollinger, M.; Bengaard, H.; Hammer, B.; Sljivancanin, Z.; Mavrikakis, M.; Xu, Y.; Dahl, S.; Jacobsen, C. J. H. *J. Catal.* **2002**, *209*, 275.

final-state energies reflects the fundamental similarity in the transition-state structures and suggests that $O_2$ dissociation kinetics on alloy surfaces can be estimated from the binding energy of atomic oxygen alone, which can be calculated more easily than the entire reaction path. Accordingly, this simple correlation opens the new possibility of using affordable theoretical methods to screen for and design better $O_2$ activation catalysts.

## Conclusions

The adsorption and dissociation of $O_2$ on Pt(111), 2%-compressed Pt(111), Pt₃Co(111), Pt₃Fe(111), and the corresponding monolayer Pt skins on the alloys have been studied using periodic self-consistent DFT (GGA-PW91) calculations in an effort to contribute some insights into the superior activities of several Pt−base metal alloys, including Pt−Co and Pt−Fe, for the ORR. Despite being significantly diluted by neighboring Pt atoms, the Co atoms on the Pt₃Co(111) surface allow $O_2$ to dissociate more easily than on Pt(111) (the smallest activation energy on Pt₃Co(111) is 0.24 eV/$O_2$, compared to 0.77 eV/$O_2$ on Pt(111)) and also bind O and $O_2$ more strongly ($-4.29$ eV/O vs $-3.88$ eV/O, $-0.92$ eV/$O_2$ vs $-0.62$ eV/$O_2$). However, Co atoms may be easily lost from the alloy surface during fuel cell operation or because of annealing so that the surfaces of alloy catalyst particles become covered by Pt only. We find a monolayer Pt skin on top of Pt₃Co(111) the least reactive surface in our study, in terms of both O and $O_2$ binding energy ($-3.50$ eV/O and $-0.34$ eV/$O_2$, respectively) and $O_2$ dissociation barrier (0.93 eV/$O_2$). If the Pt skin grows to multilayer thickness, its properties are expected to approach that of a pure 2%-compressed Pt surface, which is more reactive than the monolayer Pt skin (with $E_b^O = -3.63$ eV/O and $E_a = 0.89$ eV/$O_2$ for $O_2$ dissociation) but is, in agreement with previous findings regarding surface strain, less reactive than the equilibrium Pt surface. Mostly identical results are obtained for Pt₃Fe(111) and its Pt skin surface. The reduced reactivity of the 2%-compressed Pt surface and the Pt skins can be rationalized as due primarily to the lowering of the d-band center from the Fermi level. We propose that thin Pt skins, though less reactive than pure Pt for $O_2$ dissociation, are nonetheless more active toward the ORR because they are less poisoned by O and because they facilitate the activation of O and O-containing intermediates in bond-making elementary reaction steps in the ORR mechanism. The Pt skins also bind CO less strongly than pure Pt does, indicating that they may be more resistant to CO poisoning, a problem relevant to direct methanol fuel cells.